Indian Journal of Engineering & Materials Sciences
Vol. 32, June 2025, pp. 307-312
DOI: 10.56042/ijems.v32i03.15490

# Investigation of an electroplated $Ni_xFe_y$ film for magnetometer applications

Aditi[a,b*], Supriyo Das[a] & Ram Gopal[a,b]
[a]Central Electronics Engineering Research Institute, Pilani 333 031,India
[b]Academy of Scientific and Innovative Research (AcSIR), Ghaziabad 201 002, India

*Received: 03 December 2024; accepted: 11 April 2025*

This paper has investigated the development of a microelectromechanical system (MEMS)-based magnetometer utilizing the ultraviolet-lithographie, galvanoformung, abformung (UV-LIGA) technique, with a structural layer composed of nickel-iron (NixFey) alloy. Earlier implementations of MEMS magnetometers using pure nickel as a structural material have encountered challenges due to high residual stress, which has led to performance degradation and mechanical instability. To address this, an optimized composition of Ni (87%) and Fe (13%) has been employed to minimize residual stress and enhance the structural integrity of the device. The proposed magnetometer has been fabricated on a boro-float glass substrate, which has been chosen for its low parasitic capacitance and reduced requirement for passivation layers. The design has incorporated a novel resonant structure with support arms positioned at the extreme ends of the beam, maximizing the overlap area between movable and fixed electrodes for improved sensitivity. The device has operated based on Lorentz force transduction, where an excitation current applied at the resonant frequency has interacted with an external magnetic field, inducing vibrations. Extensive experimental investigations have been conducted to optimize the electroplating process and reduce stress. Elemental analysis of the NiFe film has been performed using energy dispersive spectroscopy (EDS) to verify the composition. The mechanical sensitivity of the device has been measured as 237 pm/Gauss at atmospheric pressure using a Laser Doppler Vibrometer (LDV), demonstrating its high-performance capabilities. This work has reported a novel MEMS-based Lorentz force magnetometer with $Ni_{87}Fe_{13}$ as the structural layer, fabricated using the UV-LIGA process. The study has established a reliable methodology for the development of stress-free, high-sensitivity magnetic sensors, contributing to advancements in miniaturized sensing technologies for applications in navigation and industrial automation.

**Keywords:** EDS, Lorentz force, MEMS Magnetometer, Ni, NiFe, UV-LIGA

## 1 Introduction

The demand for magnetic field sensors has witnessed an exponential increase over the past decade, driven by their critical applications across diverse sectors such as automotive, consumer electronics, aerospace, and medical fields[1-3]. These sensors play a pivotal role in numerous applications, including position sensing, navigation, non-destructive material testing, vehicle detection, mineral prospecting, gradiometry, brain function mapping, and advanced imaging techniques like magnetic resonance tomography[4-7]. The wide range of sensitivity and performance requirements across these applications necessitates the design and development of magnetic sensors tailored using the most suitable technologies available[8].

MEMS-based magnetometers have emerged as a promising alternative to conventional magnetic field sensors, such as fluxgate and search coil magnetometers, due to their potential for miniaturization, cost-effectiveness, and compatibility with modern microfabrication techniques[9-10]. In contrast, conventional magnetometers often require complex fabrication involving magnetic cores and coils, which limits their scalability and integration[11]. Lorentz force-based magnetic sensors offer a significant advantage by leveraging the fabrication technologies widely used for inertial sensors like accelerometers and gyroscopes, including electroplating, silicon micromachining, and wafer bonding.

Among the various methods to realize MEMS-based magnetometers, the UV-LIGA process stands out due to its flexibility in material selection and precision in microstructure fabrication. This process enables the electroplating of a variety of materials, which can be strategically used in combination with sacrificial and structural layers to achieve optimized sensor designs. For Lorentz force magnetic sensors, the use of conducting materials in the structural layer is a key requirement. Nickel (Ni) and its alloys, owing to their excellent mechanical and magnetic properties, have been extensively employed in such

*Corresponding author (E-mail: aditi.ceeri@csir.res.in)

applications[12-13]. Besides, materials with high saturation magnetization and low coercivity are also used for electromagnetic devices like inductor cores and recording heads[14]. As reported in[15] the residual stress in the Ni xylophone structure was high leading to the lower displacement at the center. Therefore, achieving low residual stress in the structural layer is essential to enhance the sensor's performance and reliability.

In this work, we report the design and fabrication of a Lorentz force-based MEMS magnetometer utilizing a NiFe alloy as the structural layer, optimized to minimize residual stress and eliminate stiction-related issues. An alloy composition of Ni (87%) and Fe (13%) was identified as optimal for achieving high mechanical stability and performance. The sensor was fabricated using UV-LIGA technology on a borosilicate glass substrate, which offers the advantages of reduced parasitic capacitance and eliminates the need for an oxidation step for passivation. It utilizes three masks for the fabrication of the sensor.

The operation of the proposed magnetometer is based on the interaction between an excitation current applied at the resonant frequency of the beam and an externally applied magnetic field by a permanent magnet. This interaction generates a Lorentz force orthogonal to the microstructure, inducing vibrations that result in capacitance changes between movable and fixed electrodes. The use of NiFe as a structural layer with minimized residual stress ensures a straight-released structure. Electroplating was performed at a low current density (5 mA/cm²) .The fabricated device was tested for its Lorentz force operation using a laser Doppler vibrometer (LDV) in the presence of a magnetic field generated by a permanent magnet. This work represents a novel approach to Lorentz force-based MEMS magnetometers, demonstrating the potential of UV-LIGA technology and NiFe alloys in advancing magnetic sensor design. This paper presents the realization, characterization, and testing of the proposed MEMS magnetic sensor, highlighting its advantages and potential applications. The findings pave the way for the development of compact, high-performance magnetic sensors for a broad range of emerging applications.

## 2 Materials and Methods

### 2.1 Design and simulation

A resonant structure with support arms positioned at extreme ends of the beam is proposed and illustrated in Fig. 1. The support arms are anchored to provide mechanical stability. For a xylophone structure of the same length, the placement of the support arms at the extreme ends significantly increases the overlap area with the bottom electrode, enhancing the device's sensitivity by maximizing the capacitance variation during operation.

An excitation current is applied along the x-direction through the support arms, while an external magnetic field is applied in the y-direction, generating a Lorentz force in the out-of-plane (z-direction). This force induces oscillations in the z-direction, where the displacement is directly proportional to the magnitude of the Lorentz force. To achieve optimal performance, it is critical to carefully design and optimize the dimensions of the structure.

The design and optimization process was conducted through Finite Element Method (FEM) simulations using COMSOL Multiphysics®. Modal analysis was performed to determine the mechanical resonant frequency of the structure, which is crucial for the device's operation. NiFe was selected as the structural layer. The meshing of the structure was achieved using tetrahedral elements, ensuring accurate simulation results. Boundary conditions were applied to fix the extreme ends of the support arms, representing the physical constraints of the device. The first mode of vibration, which corresponds to the resonant frequency of the structure, 50.8 kHz is depicted in Fig. 2. This analysis highlights the

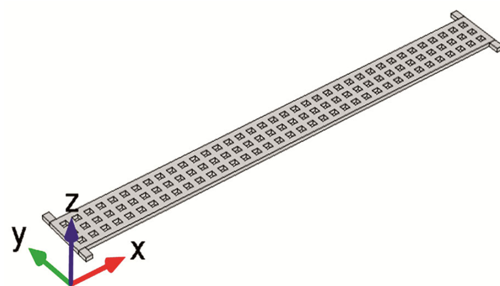


Fig. 1 — Schematic of the device.

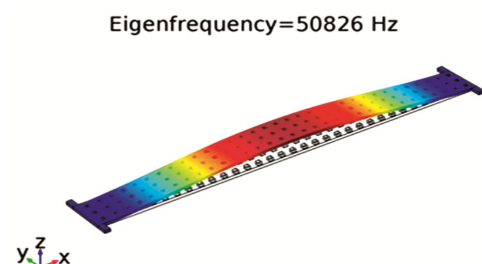


Fig. 2 — First resonant mode of the structure at 50.826 kHz.

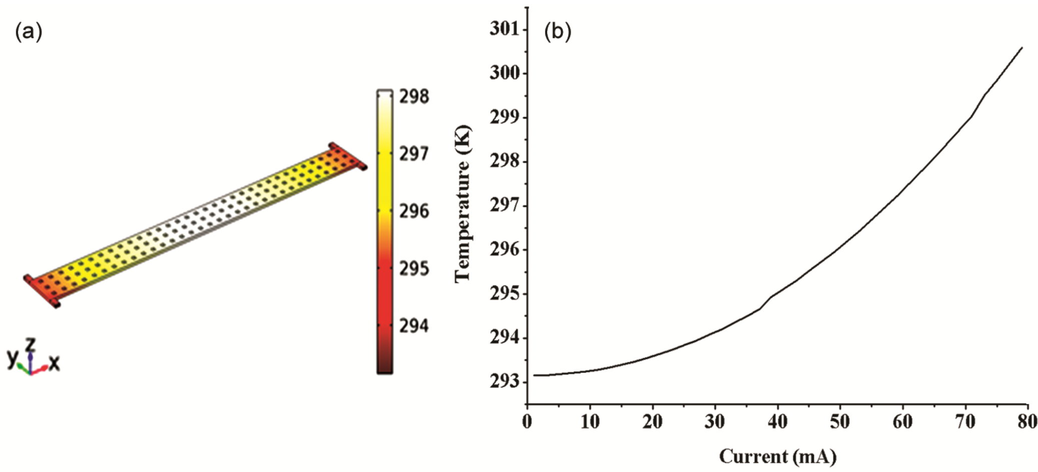


Fig. 3 — (a) The thermal gradient at 65 mA of applied current and (b) Rise in temperature with applied current.

vibrational behavior and establishes the operational parameters of the proposed sensor.

For Lorentz force transduction, an alternating current (AC) is applied at the clamped boundary in the x-direction at the resonant frequency of the device. The resulting deflection of the resonant structure is proportional to the applied current and the external magnetic field. However, the Joule heating effect is a critical limiting factor for the maximum current that can be applied to the microstructure. The heating caused by the current flow leads to thermal expansion, which induces stresses and can result in buckling of the structure. To ensure safe operation, the limiting current is defined as the current at which the device exhibits a temperature rise of 5 K above room temperature (293 K). Thermal analysis shows that the temperature gradient peaks at the center of the structure when a maximum current of 65 mA is applied, as depicted in Fig. 3a. Fig. 3b illustrates the temperature rise as a function of the drive current. To address thermal and mechanical challenges, perforations are introduced in the structural layer for two primary reasons: (a) To enable complete etching of the sacrificial layer during fabrication. (b) To reduce squeeze-film damping, thereby enhancing the dynamic response of the structure[16].

Comparative analysis under identical ambient conditions shows that the perforated structure exhibits better performance with higher deflection compared to the non-perforated one. The optimized dimensional parameters obtained from the simulations are summarized in Table 1. These parameters ensure the structural and operational reliability of the device while maintaining optimal performance characteristics.

Table 1 — Design parameters.

| Parameter | Dimension (μm) |
|---|---|
| Beam Length | 600 |
| Beam Width | 56 |
| Support Length | 15 |
| Support Width | 8 |
| Thickness | 4.5 |
| Gap | 3 |
| Bottom electrode thickness | 0.25 |
| Hole | 6 x 6 |

### 2.2 Fabrication

The fabrication of the Lorentz force-based MEMS magnetometer was carried out on a 2-inch boro-float glass substrate. The advantages of using a glass substrate include (a) Elimination of oxide growth step. Unlike silicon substrates, the insulating property of glass negates the need for a 1 μm thermal oxide layer before seed layer metallization. (b) Reduced parasitic capacitances: Glass substrates inherently have lower parasitic capacitances compared to silicon. (c) Cost-effectiveness: Glass is less expensive than silicon, making it a more economical choice for large-scale fabrication.

The process flow, illustrated in Fig. 4, involves three main fabrication steps using three lithographic masks, as described below:

#### *2.2.1 Bottom electrode and contact formation*

The process began with the preparation of the glass substrate, which was cleaned using degreasing agents followed by a piranha solution to ensure a contaminant-free surface. Subsequently, a Cr/Au bilayer (200 Å/2000 Å) was deposited using a sputtering system (VST) to form the bottom electrode and contact pads. Mask 1 was employed to define the

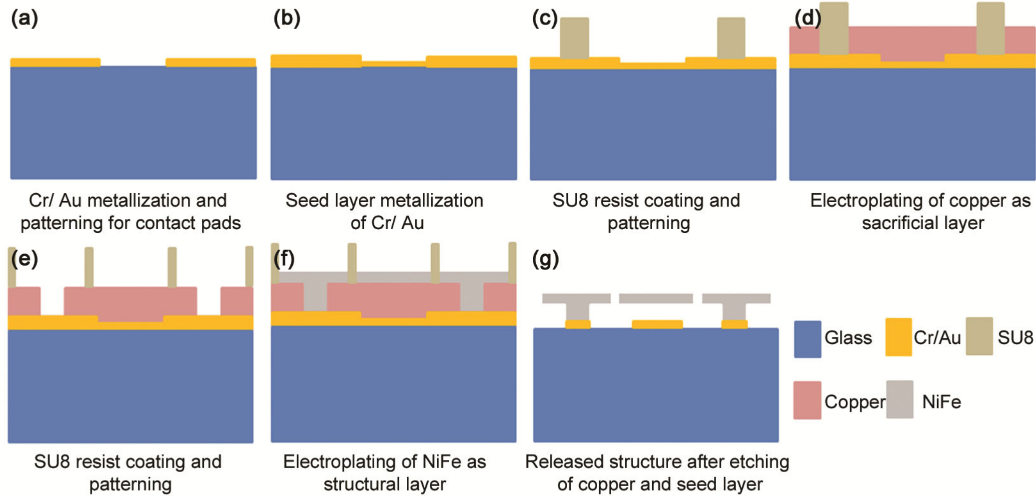


Fig. 4 — Fabrication process flow using a boro-float glass substrate.

Table 2 — Design Parameters.

| Parameter Constituents | Value |
|---|---|
| Nickel sulfate ($NiSO_4$. $6H_2O$) | 200 g/L |
| Nickel Chloride ($NiCl_2$. $6H_2O$) | 5 g/L |
| Iron Sulfate ($FeSO_4$ .$7H_2O$) | 16 g/L (Composition 1)<br>7 g/L (Composition 2) |
| Boric Acid ($H_3BO_3$) | 25 g/L |
| Saccharin ($C_7H_4NNaO_3S$. $2H_2O$) | 3 g/L |

metal pattern for the bottom electrode and contact pads, as shown in Fig. 4a. After patterning, a seed layer of Cr/Au (200 Å/2000 Å) was deposited, as shown in Fig. 4b, which served as the foundation for subsequent electroplating steps.

***2.2.2 Sacrificial layer definition***

To create the sacrificial layer, Mask 2 was utilized for patterning SU-8 photoresist. The SU-8 was selectively retained only at the anchor points, as shown in Fig. 4c, while the rest was removed. The thickness of the copper sacrificial layer determines the gap height between the bottom and top electrodes. Electroplating was performed to deposit a 3 µm-thick Cu layer, ensuring precise cavity height. The electroplated copper pattern is depicted in Fig. 4d.

***2.2.3 Structural layer definition***

Following the removal of SU-8, the structural layer was defined using Mask 3. The SU-8 was patterned to create the mold for the structural layer, as shown in Fig. 4e. The Ni-Fe alloy was then electroplated as a structural layer onto the patterned seed layer using the electrolyte composition 1[17] (as detailed in Table 2). The electroplated Ni-Fe alloy layer is depicted in Fig. 4f. The SU-8 was subsequently removed using a PG remover, with any residual material eliminated

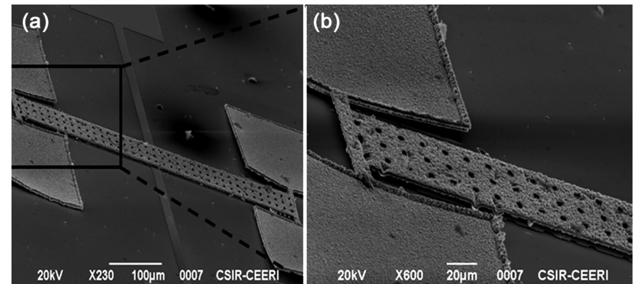


Fig. 5 — (a) SEM micrograph of fabricated structure (composition 1) and (b) Magnified view of the selected region in (a).

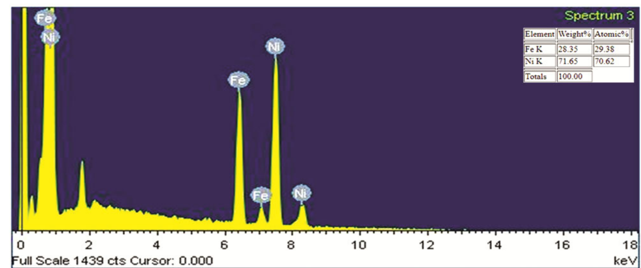


Fig. 6 — EDX of the structural layer (composition 1).

using a plasma stripper (95% $O_2$ and 5% $CF_4$). Finally, the sacrificial copper layer and the seed layer were selectively etched to release the device as shown in Fig. 4g.

***2.2.4 Material and stress optimization***

The initial fabrication results revealed that the beams were flat, but the anchors showed peeling due to high residual stress in the Ni-Fe alloy layer, as depicted in Fig. 5 (a) and magnified view in Fig. 5(b), Energy Dispersive Spectroscopy (EDS) was performed to analyze the elemental composition of the electroplated structural layer, as shown in Fig. 6.

The initial composition consisted of approximately 29% Fe and 71% Ni, which contributed to the high residual stress. The Fe content was optimized to 13%, resulting in a Ni-Fe alloy (composition 2) with significantly reduced residual stress. This optimized composition produced a flat structural layer, as confirmed by the SEM micrograph in Fig. 7(a) and magnified view in Fig. 7(b), with no buckling or peeling observed in the released device. The EDS analysis of the optimized structural layer is presented in Fig. 8.

#### *2.2.5 Electroplating conditions*

The electroplating of the Ni-Fe structural layer was carried out under controlled conditions:

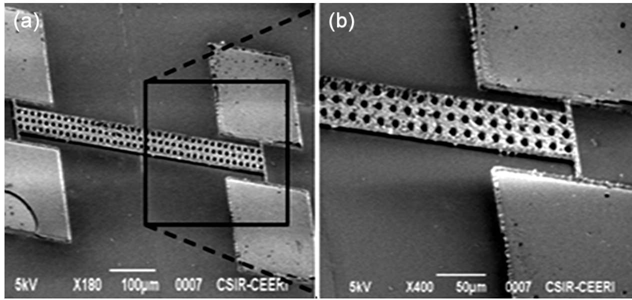


Fig. 7 — (a) SEM micrograph of fabricated structure (composition 2) and (b) magnified view of the selected region in (a).

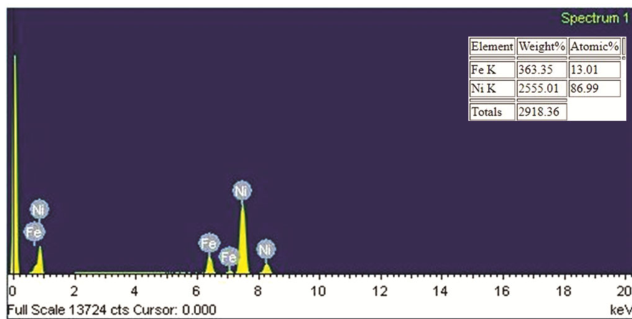


Fig. 8 — EDX of the structural layer (composition 2).

Bath temperature: Maintained at 40°C ± 1°C using a magnetic stirrer; Current density: Set to 5 mA/cm² for precise electro-deposition; Anode and cathode: Nickel was used as the anode, while the sample served as the cathode. The pH of the bath measured was 3.57; Thickness: The Ni-Fe structural layer was electroplated to a final thickness of approximately 4.5 µm.

This optimized process flow and material composition have enabled the successful fabrication of a Lorentz force-based MEMS magnetometer with minimal residual stress, as verified by SEM imaging and EDS analysis. The flat, stable structural layer demonstrates the reliability and robustness of the proposed fabrication methodology.

## 3 Results and Discussion

The released MEMS magnetometer was thoroughly tested to validate its performance. Initial testing involved determining the resonant modes using a Microsystem Analyzer (MSA-500) from Polytec for dynamic measurements. A DC bias of 1 V was applied to the bottom electrode, and a 40 mV AC excitation sweep was applied to the structural layer using a periodic chirp signal generated internally. The first mode of vibration, measured at 51.69 kHz, was experimentally observed using Laser Doppler Vibrometry via the MSA as shown in Fig. 9. This frequency closely matched the simulated value, validating the design.

Subsequently, the device's operation as a Lorentz force magnetometer was verified. An excitation current was applied at the beam's ends, between the extreme support arms, with a frequency sweep ranging from 40 kHz to 60 kHz. To measure displacement due to Lorentz force transduction, an external magnetic field of 118 Gauss was applied orthogonally to the excitation current using a

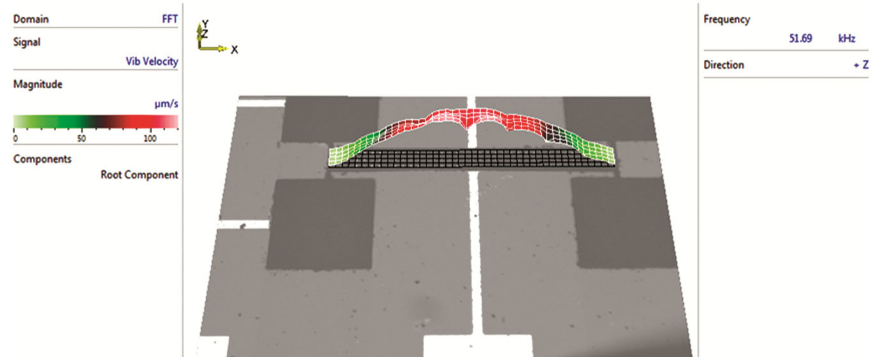


Fig. 9 — Vibration mode obtained experimentally by using LDV, primary mode at 51.69 kHz.

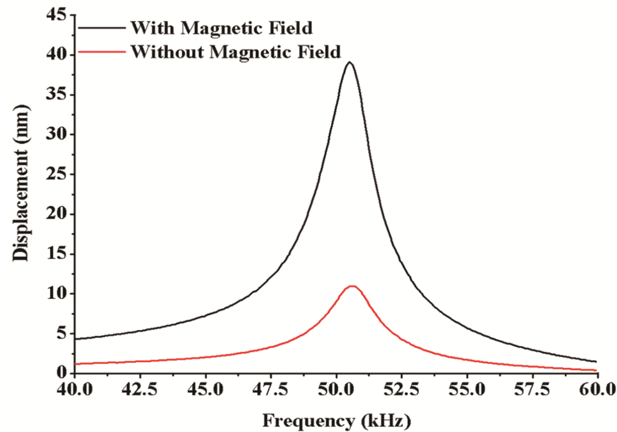


Fig. 10 — Frequency responses showing the effect of magnetic field amplitude.

permanent magnet. Fig. 10 illustrates the displacement responses of the sensor, highlighting the amplitude differences in the presence and absence of the magnetic field.

With an applied current of 4.6 mA, the device demonstrated a mechanical sensitivity of 237 pm/Gauss. These results confirm the magnetometer's effectiveness, with high mechanical sensitivity and robust design performance under the tested conditions.

## 4 Conclusion

The realization of a MEMS magnetometer using UV-LIGA fabrication technology demonstrates the potential for broader applications, including the fabrication of inertial sensors such as gyroscopes and accelerometers. The micromechanical structure was fabricated with a $Ni_{87}Fe_{13}$(87% Ni and 13% Fe) structural layer, optimized for minimal residual stress. The design incorporated resonators with support arms at the ends of the beam to maximize the overlap area, improving performance. The structural layer was electroplated at a current density of 5 mA/cm$^2$. A glass substrate was chosen instead of silicon to minimize parasitic capacitances in capacitive sensing applications. The device demonstrated a sensitivity of 237 pm/Gauss under atmospheric pressure, making it highly effective for its intended purpose. The $Ni_{87}Fe_{13}$ composition has been identified as optimal for achieving a balance between structural integrity and minimized internal stress. Future advancements could explore pulse plating at reduced current densities, which has been shown to decrease internal stress compared to conventional plating[18] while maintaining the desired thickness for magnetometer applications. This approach could further enhance the performance and reliability of such devices.

## Acknowledgements

The authors would like to acknowledge the motivation and support of the Director, CSIR-CEERI, Pilani. The authors would also like to thank the scientific and technical members of the Semiconductor Area, associated with the work carried at CSIR-CEERI, Pilani. The work was financially supported by CSIR, New Delhi, to carry out the research work.

## References


1 Aditi G, Gopal & Ram, *Microsyst Technol*, 23 (2017) 81.

2 Herrera-May A, Soler-Balcazar J, Vázquez-Leal H, Martínez-Castillo J, Vigueras-Zuñiga M & Aguilera-Cortés L, *Sensors*, 16 (2016) 1359.

3 Marra C R, Gadola M, Laghi G, Gattere G & Langfelder G, *J Microelectromech Syst*, 27 (2018) 748.

4 Zhang W & Lee J Y, *IEEE Electron Device Lett*, 34 (2013) 1310.

5 Langfelder G & Tocchio A, *IEEE Trans Magn*, 50 (2014) 4700106.

6 Dabsch A, Rosenberg C, Stifter M & Keplinger F, *J Micromech Microeng*, 27 (2017) 055014.

7 Mesa J L *et al*, *IEEE Magn Lett*, 6 (2015) 6500104.

8 Yang H H, Myung N V, Lee J, Park D Y, Yoo B Y, Schwartz M, Nobe K & Judy J W, *Sens Actuators A: Phys*, 97–98 (2002) 88.

9 Herrera-May A L, Aguilera-Cortés L A, García-Ramírez P J, Mota-Carrillo N B, Padrón-Hernández W Y & Figueras E, *Microsensors* (IntechOpen, Rijeka), ISBN: 9789533071368, 2011, 1.

10 Yin X, Jiao Q, Yuan L & Liou S, *IEEE Trans Magn*, 49 (2013) 3890.

11 Ripka P & Janosek M, *IEEE Sens J*, 10 (2010) 1108.

12 Kumar R R, Gowrisankar P, Balaprakash V, Sudha S & Manimaran E I, *J Mater Sci: Mater Electron*, 29 (2018) 11591.

13 Manimaran E I, Antonyraj K, Navaneetha E R & Rajesh P, *J Mater Sci: Mater Electron*, 29 (2018) 3715.

14 Xu J, Dai B, Ren Y, Wang Y & Huang X, *J Mater Sci: Mater Electron*, 26 (2015) 2931.

15 Rochus V, Jansen R, Rottenberg X, Tilmans H A C, Ranvier S, Lamy H & Rochus P, *Proc 13th Int Thermal, Mechanical & Multi-Physics Simulation & Experiments in Microelectronics & Microsystems (IEEE, New York)*, 2012, 1.

16 Bao M, Analysis and design principles of MEMS devices (Elsevier, Amsterdam), 1st Edn, ISBN: 9780444506697, 2005, 26.

17 Taylor W P, *Electrochem Solid-State Lett*, 2 (1999) 624.

18 Hadian S E & Gabe D R, *Surf Coat Technol*, 122 (1999) 118.